INTERNATIONAL ATOMIC ENERGY AGENCY
UNITED NATIONS EDUCATIONAL, SCIENTIFIC AND CULTURAL ORGANIZATION

INTERNATIONAL CENTRE FOR THEORETICAL PHYSICS
34100 TRIESTE (ITALY) - P.O.B. 586 - MIRAMARE - STRADA COSTIERA 11 - TELEPHONES: 224281/2/3/4/5/6
CABLE: CENTRATOM - TELEX 460392-I

SMR 115 - 58

WINTER COLLEGE ON LASERS, ATOMIC AND MOLECULAR PHYSICS

(21 January - 22 March 1985)

ATMOSPHERIC MOLECULES

C. MULLER
Institut d'Aéronomie Spatiale
de Belgique
Ave. Circulaire, 3
1180 Bruxelles
Belgium

Atmospheric molecules

- The earth's atmosphere
- Penetration of solar radiation
- Infrared spectroscopy in the atmosphere.
- Observation techniques.
- Atmospheric physics
  - meteorology
  - aeronomy: science of the physico-chemical processes of planetary atmospheres.

Specificity: - observation science
- the different phenomena are not observed separately.
- the observations are often impossible to simulate in laboratory conditions.

What will not be covered in this course!:
- the atmospheres of other planets
- the ionosphere
- the magnetosphere.

I will say a few words in lecture 2 about the scattering of light by particles.

The earth's atmosphere

Composition: 78.1 % nitrogen N_2
20.9 % O_2
1 % argon

traces of Ne, He, Kr, Xe

CO_2 : 340 ppm
H_2O : from saturation → 3 ppm
CH_4 : 1.6 ppm
H_2 : 0.5 ppm
N_2O : 0.3 ppm
O_3 : highly variable

Composition observed at ground level
these gases are in equilibrium with sea and surface waters.

Primitive atmosphere

mainly reducing: H_2, N_2, CO_2, A, CH_4, H_2O
traces of NH_3 ?

O_2 : trace gas, no relations to life

buildup : 1% O_2 : "Pasteur Point"
: 2% O_2 : ozone layer
life is possible on the continents

Physical conditions

hydrostatic equation $\rho = -\frac{1}{g}\frac{dp}{dz}$

$p = nkT$

$$\frac{dp}{p} = -\frac{dz}{kT/mg} \longrightarrow p = p_0 e^{-z/H}$$

$H = kT/mg$

H: scale height: known since Pascal and Laplace

adiabatic expansion: decrease in temperature
the observations of the 20th century lead to a different view

1900-1914 : discovery of a layer of stable temperature above 12 km.

1918-1940 : development of aviation
1930's first stratospheric soundings, discovery of an increase in temperature in the stratosphere

1946-1957 : soundings of upper atmosphere up to 100 km

1957- : soundings of atmospheric densities by artificial satellites.

1970- : observation of atmospheric properties from space

[redacted]

1954: acceptance of an international nomenclature of atmospheric regions.

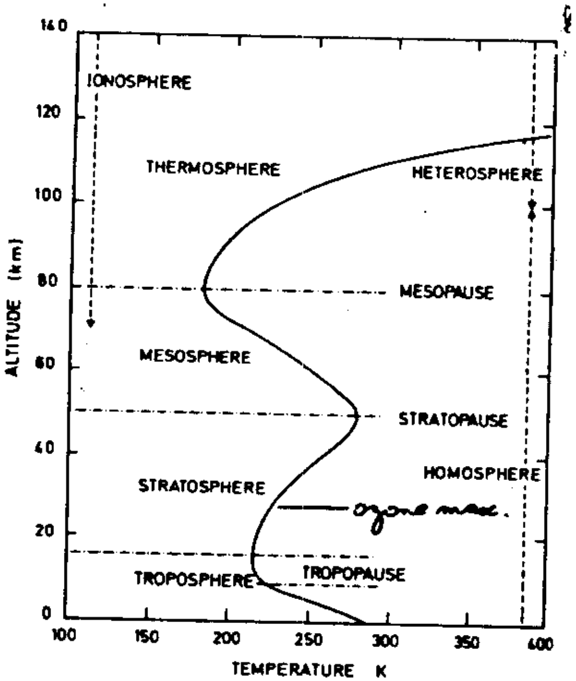

Fig. 1.1 Conventional division of the atmosphere into zones corresponding to the temperature profile; two lines are indicated at the tropopause level to show the variation between the tropical summer tropopause of about 18 km and the polar winter tropopause sometime as low as 8 km.

Chapman cycle

$$\begin{cases} O_2 + h\nu \rightarrow O + O & \lambda < 240\text{ nm} \\ O_2 + O + M \rightarrow O_3 + M & \\ O_3 + h\nu \rightarrow O_2 + O & \lambda < 310\text{ nm} \end{cases}$$

Catalytic cycles

$$NO + O_3 \rightarrow NO_2 + O_2$$
$$NO_2 + O \rightarrow NO + O_2$$
$$\overline{O_3 + O \rightarrow 2O_2}$$

$$Cl + O_3 \rightarrow ClO + O_2$$
$$ClO + O \rightarrow Cl + O_2$$
$$\overline{O_3 + O \rightarrow 2O_2}$$

If not interrupted these catalytic cycles destroy all the ozone.

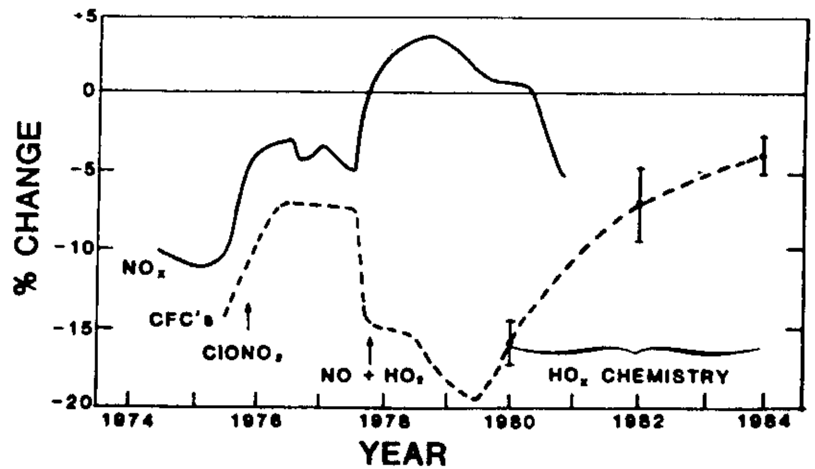

Column ozone depletion predictions from 1974 to 1984

(6)

$$\frac{\partial n(O_3)}{\partial t} = -J_{O_3} n(O_3) + k_2 n(O) n(O_2) \cdot (M)$$

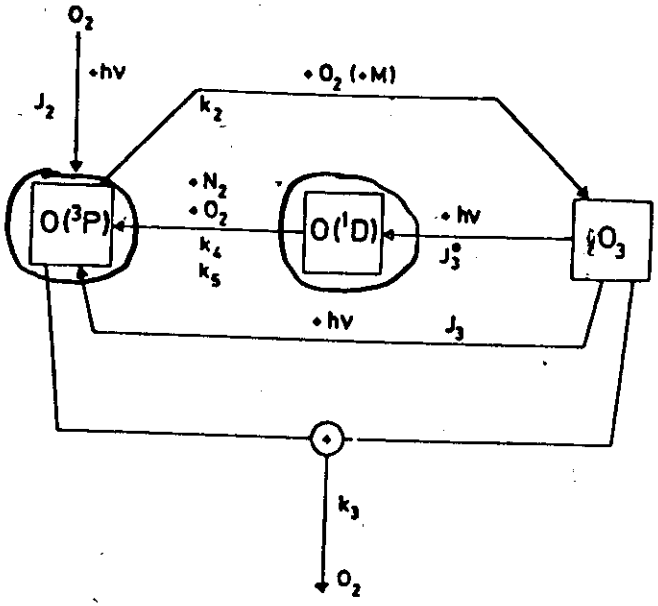

(7)

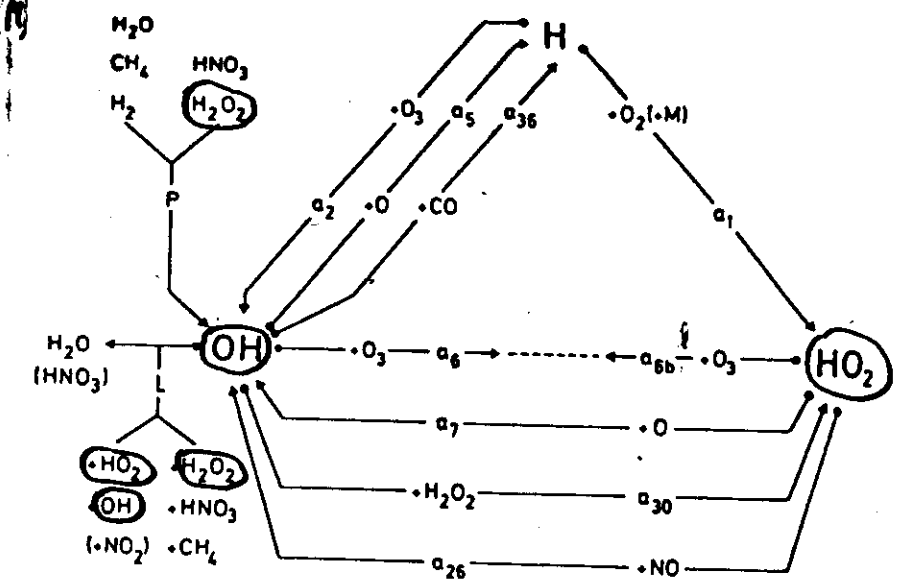

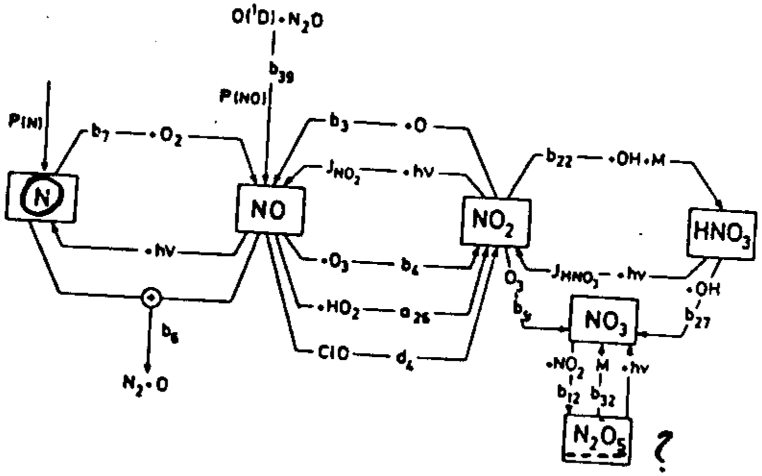

?

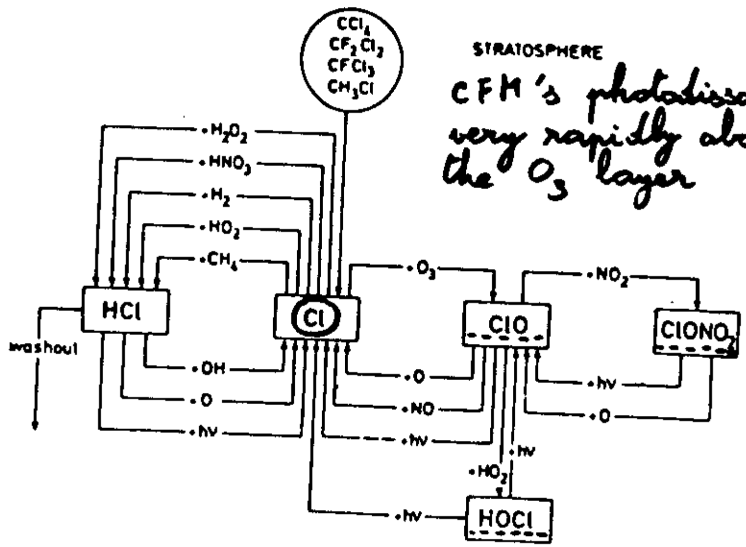

CFM's photodissociate very rapidly above the O_3 layer

What was not on these diagrams and remain to be measured?

- sulfur chemistry: OCS: detected
  SO
  SO_2
  H_2SO_4
- nitrogen chemistry: $HO_2 - NO_2$ (HNO_4)
  HNO_2
- carbon chemistry - CHOH (CH_2O) detected in troposphere
  CN containing molecules.
- components of tropospheric pollutions.

Has anything been overlooked?

yes, bromine chemistry
- CH_3Br
- $C_2H_4Br_2$
- CF_3Br
- CF_2ClBr

happily, few industrial production.

What is now happening (1985)?

- Significant increase in tropospheric ozone and rain acidity (waldsterben)
- Depletion of upper stratospheric O_3.
- Increases of CO_2, CFM's, CH_4, maybe N_2O.
- The statisticians are still unable to give a trend for total ozone at columns.

MODELING the Stratosphere

$$\frac{\partial n_i}{\partial t} + \frac{\partial \phi_i}{\partial z} = P_i - L_i$$

continuity equation

$$\phi_i = - K\, n(M) \frac{\partial f_i}{dz}$$

f_i : volume mixing ratio of the constituent

$K(z)$: diffusion coefficient (eddy diffusion)

- $\frac{\partial n_i}{\partial t} = 0$: steady state
- Requires boundary conditions for long lived species.
- The coupling of the equations come through the P_i and L_i terms.

Other type of models : 2 D models
3 D models
become close to GCM models
no present model can treat simultaneously chemistry and 3D transport.

limitation : - $K(z)$ is an empirical parameter with no relations to geophysics
- OH has never been quantitatively measured.

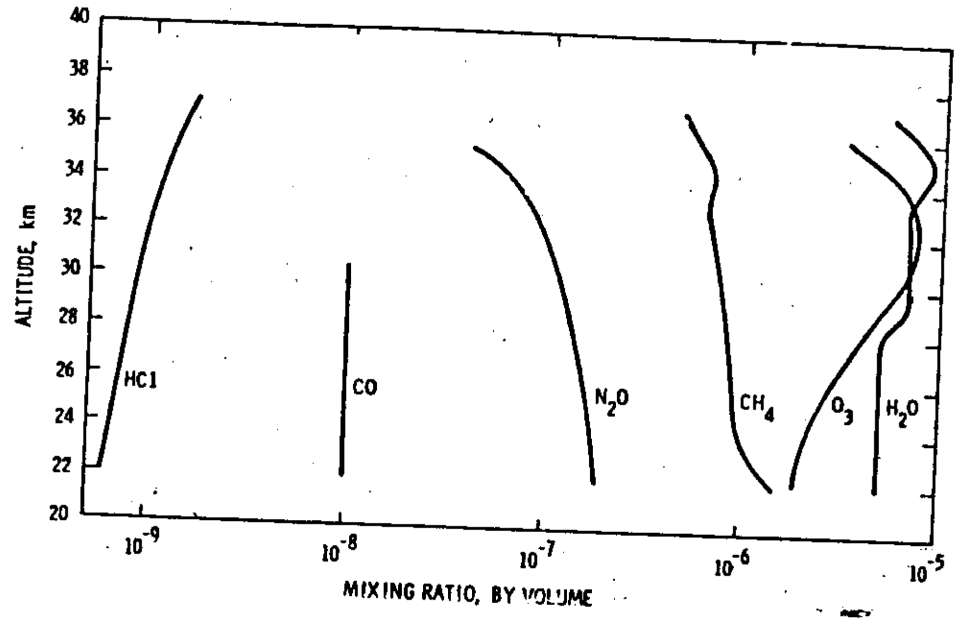

Figure 1

Farmer et al.

(10)

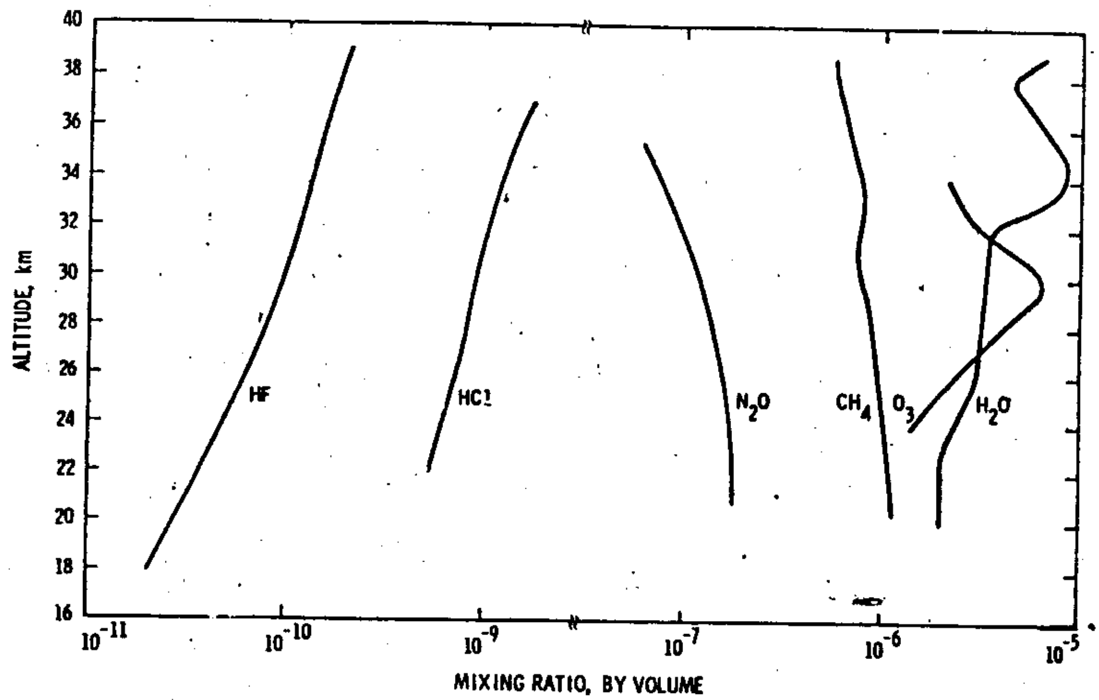

Figure 2

Farmer et al.

(11)

SPIRE Stair *et al*

Sept 28, 1977, Poker Flat Alaska.

Z = 124 km
± 5 km

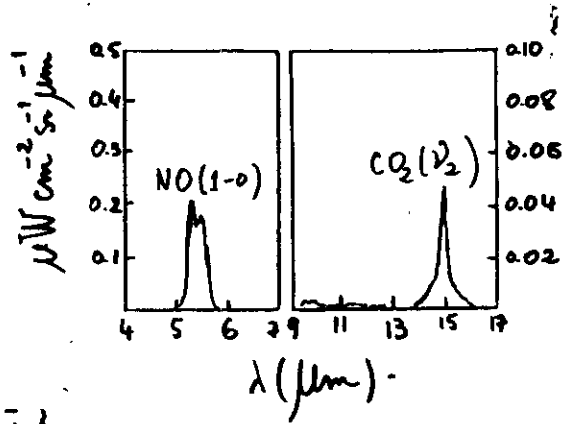

nuit.

Z = 81 km
± 5 km

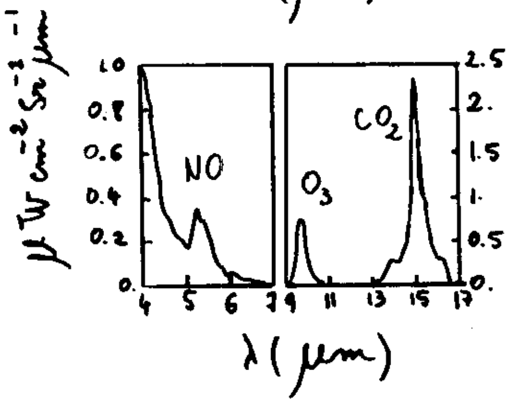

Observations aurorales : Stair *et al*.

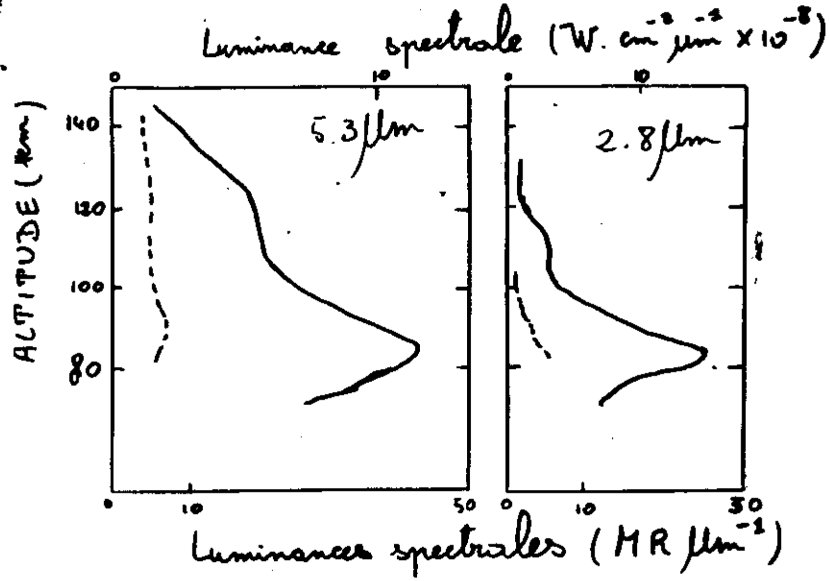

La bande 2-0 de NO n'apparait pas dans les conditions normales !

80 km

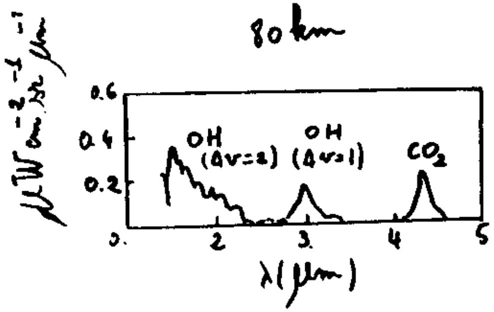

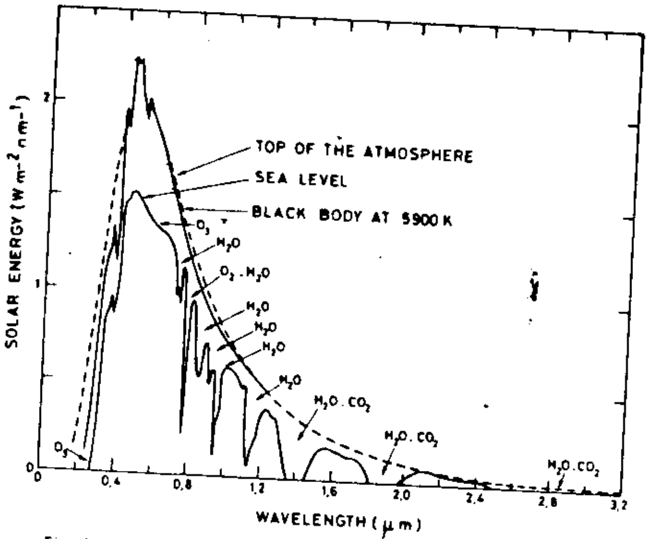

Fig. 2.1. Solar spectrum in its main energetic region compared with a blackbody spectrum and spectrum outside the atmosphere.

- the main part of the solar energy is in the visible

- minor constituents affect mostly the U.V. and I.R. parts of the spectrum

$M_E = \sigma T^4$ $\quad T = 5975\,K$

$S_E = \beta_g M_E$ dilution factor: $\beta_g = \frac{R_s^2}{4 r_s^2}$

SE = 1.96±0.02 cal/(cm² min) max in January : 6.6% var.

Lyman α : 121.6 nm

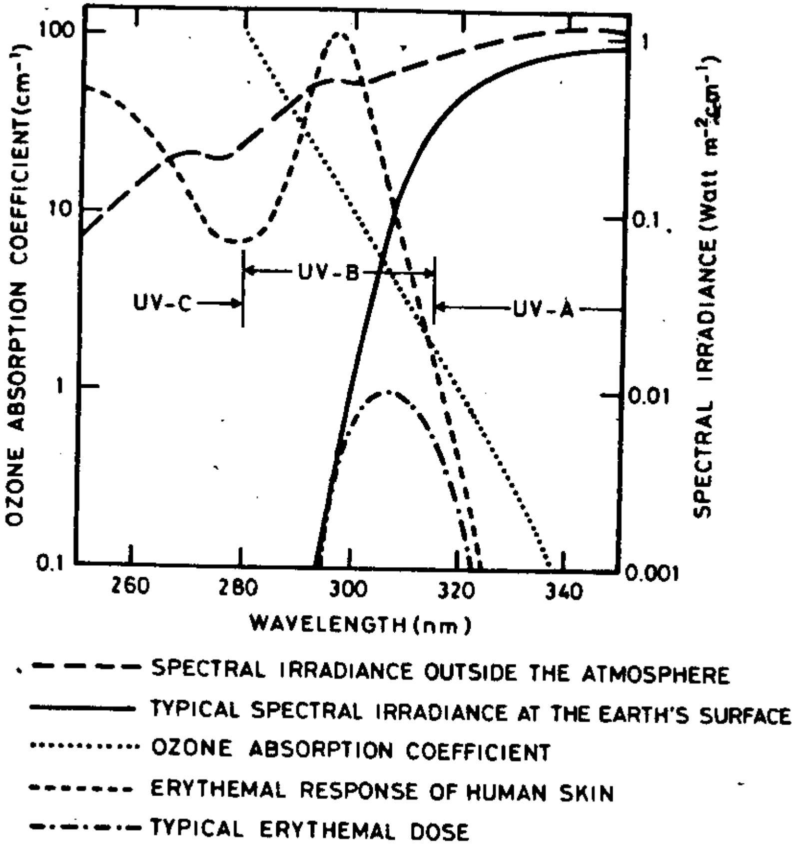

Fig. 2.2. Erythemal action of radiation compared with solar radiation at ground level and ozone spectrum.

O_3 acts as an U.V. B filter

Lyman α solar flux

3×10^{11} photons cm^{-2} sec^{-1}.

$$F_{L\alpha} = \left[1.5 + 6.3 \times 10^{-3} F_a (10.7\,cm^{-1}) + 5.4 \times 10^{-3} F_j (10.7\,cm^{-1}) \right.$$
$$\left. \times 10^{11} \text{ photons cm}^{-2} \text{sec}^{-1}\right]$$

$$F_{L\alpha} = \left[2.1 + 7.7 \times 10^{-3} R_a + 3.8 \times 10^{-2} R_j\right] \times 10^{11} \text{ phot cm}^{-2} \text{s}^{-1}$$

R_a, R_j } Wolf numbers as defined by Zürich observatory.

The other spectral domains relevant for photochemistry exhibit a similar empiricism and are accessible only to observation!

Photodissociation coefficient

O_2 in a radiation field:

$$\begin{cases} \dfrac{\partial n(O_2)}{\partial t} = -J(O_2)\, n(O_2) \\ O_2 + h\nu \rightarrow O + O \end{cases}$$

$$J_\infty = \sum j_i = \sum_i \sigma_i q_i$$

$$J(z) = \sum_i \sigma_i q_i e^{-\tau}$$

τ being the integral from ∞ to z of $\sigma n \ell$

χ: zenith distance

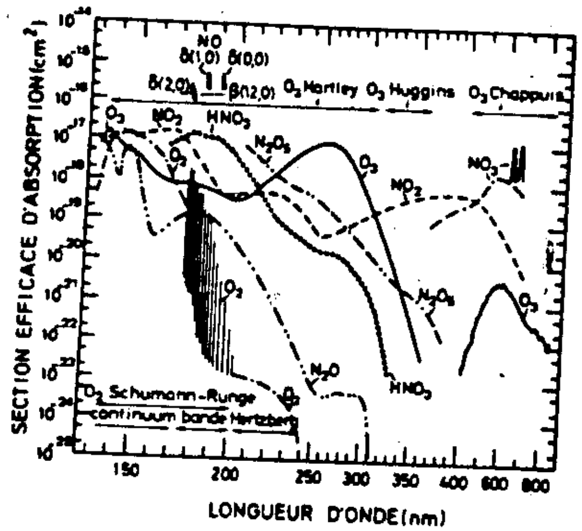

Figure 2.1. Allure du spectre des sections efficaces d'absorption, d'après Brasseur (1976).

Schumann Runge continuum: upper mesosphere
bands: down to the stratosph

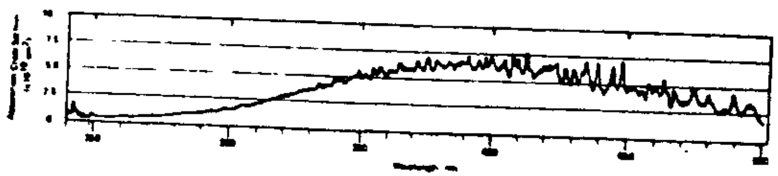

Figure 2.2. Section efficace d'absorption de NO_2, d'après Hall et Blacet (1952).

An other example: NO

NO is the main sources of ions in the D region of the ionosphere

$$NO + h\nu (Ly\alpha) \rightarrow NO^+ + e^-$$

serie of bands:

γ_{bands} : $A^2\Sigma \rightarrow X^2\Pi$

β : $B^2\Pi \rightarrow X^2\Pi$

δ : $C^2\Pi \rightarrow X^2\Pi$

ε : $D^2\Sigma \rightarrow X^2\Pi$

Photodissociation of NO:

- predissociation of (1-0) band δ at 183.2 nm
- main process but also possible from β, γ, δ and ε bands

In this case J_o must be computed for each subband

confirms: $J_o(\beta, 8\text{-}0) = 1.5 \times 10^{-7}\ sec^{-1}$

$J_o(\beta, 9\text{-}0) = 1.6 \times 10^{-7}\ sec^{-1}$

$J_o(\beta, 10\text{-}0) = 1.3 \times 10^{-7}\ sec^{-1}$

$J_o(\delta, 1\text{-}0) = 2 \times 10^{-6}$ if $T = 4700k$

$= 2.5 \times 10^{-6}$ if $T = 4650$

peuvent intervenir dans les systèmes β, γ, δ et ε absorbant à partir de l'état fondamental $X^2\Pi$ respectivement vers les états excités $A^2\Sigma^+$, $B^2\Pi$, $C^2\Pi$ et $D^2\Sigma^+$. Pour l'étude détaillée du spectre d'absorption et des différents processus intervenant dans la prédissociation (voir détails dans Heicklen et Cohen, 1968), il faut se référer (Fig. 22b) aux travaux de Callear et collaborateurs (1963-1970) et de Miescher et collaborateurs (1957-1970) avec ceux de Groth, Kley et Schurath (1971) et en tenant compte des résultats les plus récents de Mandelman et Carrington (1974), Callear (1976, com. privée) et Miescher (1975, com. privée). Une première analyse détaillée applicable à la

NO

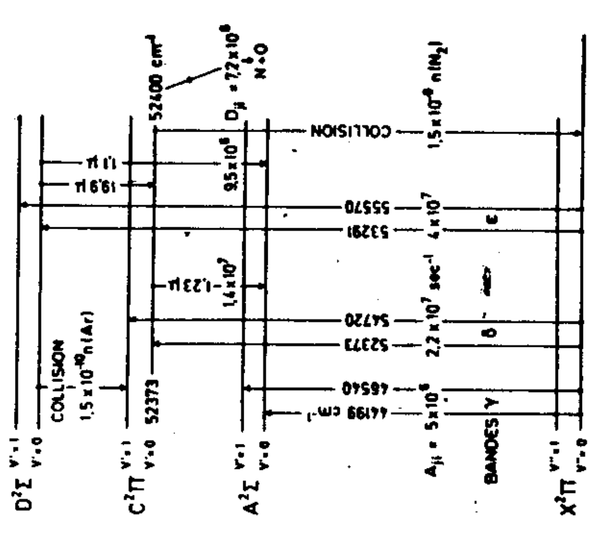

Fig. 22b. — Etats électroniques des bandes, γ, δ et ε de NO avec la probabilité d'émission correspondant à chaque état.

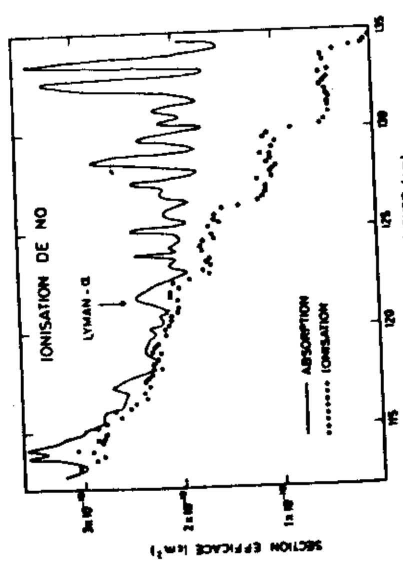

Fig. 21. — Section efficace d'absorption de NO à λ < 135 nm avec la structure de l'ionisation, en particulier à Lyman α.

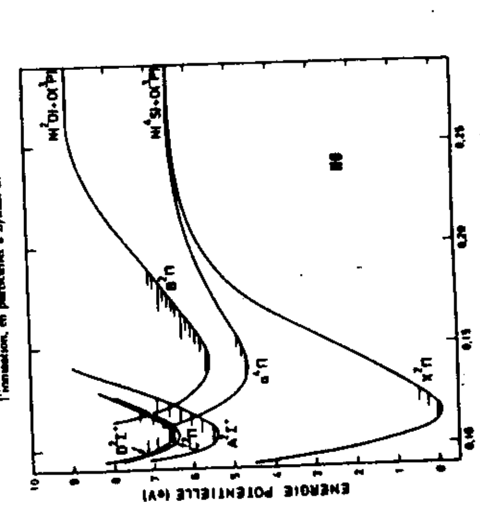

Fig. 22a. — Courbes d'énergie potentielle des états électroniques de NO correspondant aux systèmes β, γ, δ et ε.

Gaydon, 1957 ; Harris et King, 1940 ; Harris, King, Benedict et Pearce, 1940), le spectre visible et ultraviolet au-delà de 300 nm est beaucoup plus compliqué. En fait, le spectre consiste en un très grand nombre de bandes très mal définies depuis 1 μ jusqu'à environ 400 nm où l'analyse de l'une ou l'autre bande commence seulement (Douglas et Huber, 1965 ; Stevens et Zare, 1975 ; Brand, Chan et Hardwick, 1975). C'est pourquoi l'interprétation spectrale est difficile (par exemple, Gangi et Burnelle, 1971 ; Jackels et Davidson, 1976).

En simplifiant, on peut dire aujourd'hui qu'il suffit de considérer la limite supérieure de photodissociation à λ = 398 nm (Douglas et Huber, 1965 ; Uselman, 1975 ; Uselman et Lee 1976a). Elle est fixée par le caractère marqué de prédissociation de raies de rotation. Ce processus correspond à

$$NO_2 + h\nu\ (\lambda < 398{,}0\ nm) \rightarrow NO(^2\Pi) + O(^3P) \qquad (66)$$

alors que l'atome excité d'oxygène $O(^1D)$ ne peut apparaître qu'à λ < 244 nm comme l'indique d'ailleurs le spectre observé par Harris (1928) et par Ionescu (1937) avec des bandes diffuses à des longueurs d'onde inférieures à 245 nm. D'après les expériences les plus récentes (Uselman, 1975 ; Uselman et Lee, 1976b), la photodissociation

$$NO_2 + h\nu\ (\lambda < 244\ nm) \rightarrow NO(^2\Pi) + O(^1D) \qquad (67)$$

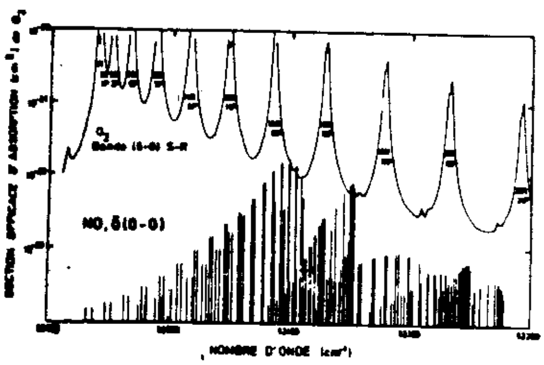

Fig. 24. — Distribution des raies de la bande δ (0—0) de NO à 270 K en présence de celle de la bande (5—0) du système de Schumann-Runge de O_2.

170

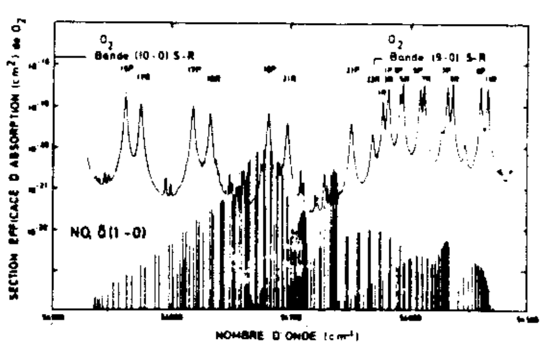

Fig. 25. — Distribution des raies de la bande (1—0) de NO à 270 K en présence de celle des bandes (10—0) et (9—0) du système de Schumann-Runge de O_2.

n'apparaît qu'avec une efficacité de 0,5 ± 0,1. La photodissociation (66) donnant des atomes $O(^3P)$ intervient encore, à moins que l'on envisage la possibilité du processus

$$NO_2 + h\nu\ (\lambda < 275\ nm) = N(^4S) + O_2(^3\Sigma_g^-) \qquad (68)$$

Cette dernière possibilité n'a pas été considérée par Preston et Cvetanovic (1966) lors de leur étude de la photodissociation à λ = 229 nm.

A des longueurs d'onde plus courtes, on peut encore introduire le processus suivant

$$NO_2 + h\nu\ (\lambda < 167\ nm) = NO(^2\Pi) + O(^1S) \qquad (69)$$

comme l'ont indiqué Nakayama, Kitamura et Watanabe (1959).

Au-delà de 148 nm, Mori (1955) avait déjà détecté une prédissociation qu'il avait attribuée à une dissociation de NO_2 avec NO dans un état excité. En fait, dans l'ultraviolet lointain, Welge (1966) a observé les processus suivants avec diverses lampes (krypton 116,5 et 123,6 nm ; xénon 129,5 et 147 nm)

$$NO_2 + h\nu\ (\lambda < 129{,}5\ nm) \rightarrow NO(A\ ^2\Sigma^+ ;\ v = o) + O(^3P) \quad (70)$$

et

$$NO_2 + h\nu\ (\lambda \leq 129{,}5\ nm) \rightarrow NO(B\ ^2\Pi ;\ v = 0, 1, 2, 3) + O(^3P). \quad (71)$$

171

(20)

10

(21)

Maxwell equations

$$\vec{\nabla}\times\vec{E} = -\frac{\partial \vec{B}}{\partial t} \qquad \vec{\nabla}\cdot\vec{J} + \frac{\partial \vec{\nabla}\cdot\vec{D}}{\partial t} = 0$$

$$\vec{\nabla}\times\vec{H} = \frac{\partial \vec{D}}{\partial t} + \vec{J} \qquad \vec{\nabla}\cdot\vec{B} = 0$$

$$\vec{B} = \mu\mu_0 \vec{H}\ ,\quad \vec{D} = \varepsilon\varepsilon_0\vec{E}\ ,\quad \vec{J} = \sigma\vec{E}$$

without any hypothesis

$$\vec{E} = \frac{\vec{z}\ c_z}{2}\left[\cos(kz+\omega t) - \cos(kz-\omega t)\right]$$

$$\beta = kz + \omega t \ :\ \text{independant of } x \text{ and } y$$

$$u = \frac{dz}{dt} = \pm\frac{\omega}{k} = \pm\frac{1}{\sqrt{\mu\mu_0\varepsilon\varepsilon_0}}$$

$$c = \frac{1}{\sqrt{\varepsilon_0\mu_0}}$$

$$n = \frac{c}{u} = \sqrt{\mu\varepsilon} \Rightarrow n \geq 1$$

direction of $\vec{E}$: polarisation.
- random : unpolarized
- varies or rotates with frequency ω.

if $\vec{E} = \vec{x} E_0 \cos(kz-\omega t)$
then $\vec{H} = \vec{y}\,\sqrt{\frac{\varepsilon\varepsilon_0}{\mu\mu_0}}\, E_0 \cos(kz-\omega t)$

energy expressed by $\vec{S} = \vec{E}\times\vec{H}$

A step further...

$\vec{E} \approx e^{-i\omega t} \quad \vec{H} \approx e^{-i\omega t}$

$\mu \approx 1$

we introduce in Maxwell's equations...

$$\vec{E} = \vec{e}\, E_0 \exp\left\{ i \left[\left(\varepsilon + \frac{i\sigma}{\varepsilon_0 \omega} \right)^{1/2} k_0 z_1 - \omega t \right] \right\}$$

$$m = \left(\varepsilon + \frac{i\sigma}{\varepsilon_0 \omega} \right)^{1/2} = m_1 + i m_2$$

$$\vec{E} = \vec{e}\, E_0 \exp(-m_2 k_0 z) \exp\left[i (m_1 k_0 z - \omega t) \right]$$

absorption ($\exp(-m_2 k_0 z)$) — propagation (m_1)

$$\beta = m_1 k_0 z - \omega t$$

phase velocity: $\frac{c}{m_1}$

dielectrics $\sigma \to 0$ $m_2 \to 0$

conductors $\sigma^2 / \varepsilon^2 \varepsilon_0^2 \omega^2 >> 1$

$$m_1 \approx m_2 \approx \sqrt{\frac{\sigma}{2 \varepsilon_0 \omega}}$$

$$\vec{S} = \frac{1}{2} \mathrm{Re} \left(\vec{E} \times \vec{H}^* \right)$$

And now scattering...

far from a scattering center

$$\frac{d^2 \psi}{dr^2} + \frac{2}{r} \frac{d\psi}{dr} + k_0^2 \psi = 0$$

solution: $\psi = \psi_0 \, e^{i k_0 r} / r$

$$\vec{E}_{sca} = \frac{e^{i k_0 r}}{k_0 r} \left(S_1 \right) \vec{E}_{inc}$$

$$\begin{pmatrix} E_{H,sca} \\ E_{V,sca} \end{pmatrix} = \frac{e^{i k_0 r}}{k_0 r} \begin{pmatrix} S_2 & S_3 \\ S_4 & S_1 \end{pmatrix} \begin{pmatrix} E_{H,inc} \\ E_{V,inc} \end{pmatrix}$$

isotropic medium: $S_3 = S_4 = 0$

otherwise: birefringence.

and a step beyond some of the longest calculations of classical physics:

Mie scattering

$$S_1 = \sum_{n=1}^{\infty} \frac{2n+1}{n(n+1)} \left[a_n \pi_n + b_n \tau_n \right]$$

$$S_2 = \sum_{n=1}^{\infty} \frac{2n+1}{n(n+1)} \left[b_n \pi_n + a_n \tau_n \right]$$

π and τ related to the Legendre polynomials

$\pi_1(\alpha) = 1 \quad \tau_1 = \cos\alpha$

$\pi_2(\alpha) = 3\cos\alpha \quad \tau_2 = 3\cos 2\alpha$

a_n and b_n are expressed in terms of Bessel functions and need specific computation!

[redacted]

Radiative transfer

in the case of L.T.E.

$$dI = B\,k\,\rho\,dz$$

$$B = \sigma T^4$$

absorption : $dI = -I\,k\,\rho\,dz$

balance : $dI = B\,k\,\rho\,dz - I\,k\,\rho\,dz$

Schwartschild equation.

This balance must be computed locally in optically thin layers which will be coadded!

if the equation for absorption in integrated : $dI = -I\,k\,n\,l\,dz$

$$I = I_0\,e^{-knl}$$

Main modifications to the balance:

changes in
- $n(CO_2)$
- $n(CH_4)$
- $n(N_2O)$
- $n(CFM's)$

(24) (25) 5

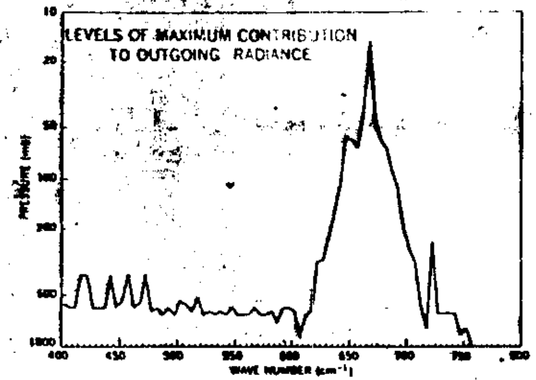

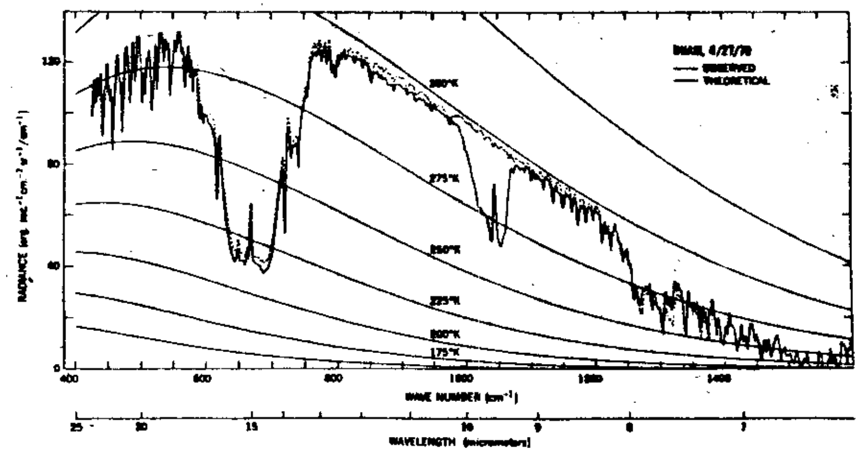

Fig. 3. Comparison of observed and theoretical radiances for a clear atmosphere near Guam at 15.1°N and 215.3°W on April 27, 1970.

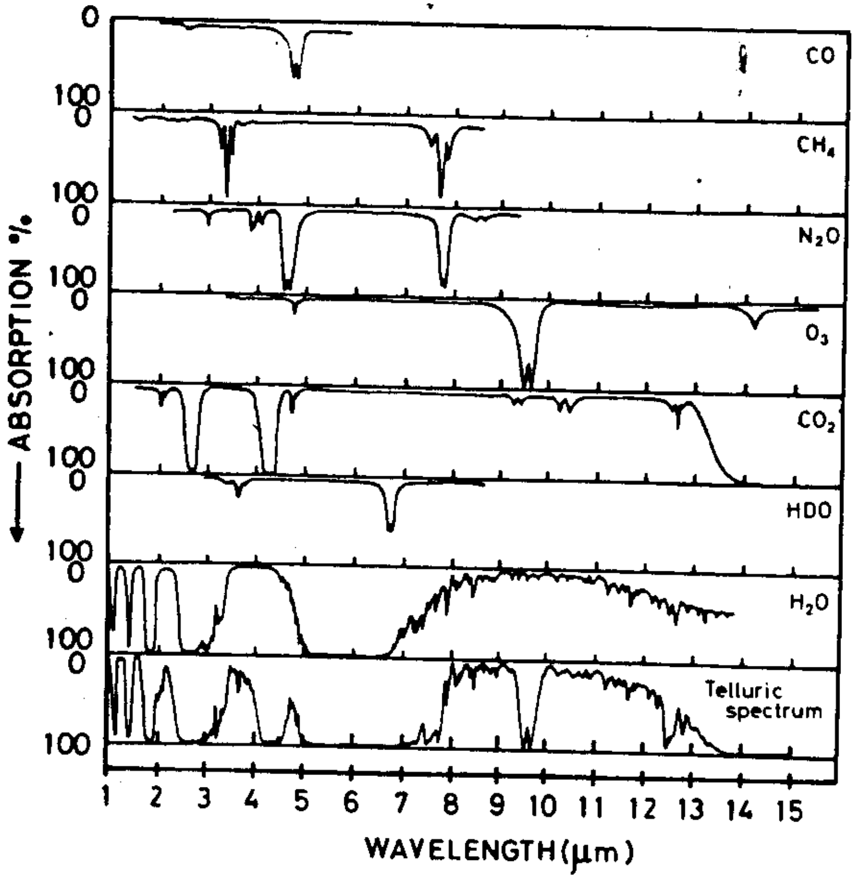

Fig. 2.3. Representation of the telluric infrared transmission spectrum, the atmospheric windows and absorptions of the main gases are clearly represented.

how to describe a spectrum?

- signature : spectral transmittance or reflectances as a function of wavelength often partly if not purely empirical !
- band : absorption corresponding to the transition between two vibrational states
- branch : set of a band corresponding to a particular ΔJ of the main rotational quantum number
- line : transition between two completely defined states (rotation, vibration, spin, etc ...)

the line is entirely defined by

position : F
intensity : S
energy of the lower level : E''
Lorentz half-line width : α_L

MOLECULAR INTERACTIONS

$$E = E_t + \underset{\sim}{E_v} + \underset{\sim}{E_r} + E_e + E_s$$

$$E_r \simeq B J(J+1) + D J^2 (J+1)^2 + \dots$$

$$B = \frac{\hbar}{4\pi I} \quad \text{diatomic}$$

$$E_r \simeq B J(J+1) + (A-B) k^2 + \dots$$

$$A = \frac{\hbar}{4\pi I_a} \quad \text{symmetric top}$$

$$E_r = \left(\frac{B+C}{2}\right) J(J+1) + \left(A - \frac{B+C}{2}\right) w$$

$$w = K^2 + c_1 b_p + c_2 b_p^2 + c_3 b_p^3$$

$$b_p = \frac{C-B}{2A-B-C} \qquad B \simeq C$$

$$b_o = \frac{A-B}{2C-B-A} \qquad A \simeq B$$

(asymmetric)

Spherical tops : CH_4, CF_4 — 19 quantum numbers !!!

The rotational energies give the position of microwave lines.

$$F = E' - E''$$

The position of rotation-vibration lines is given by taking into account the energy difference between vibrational states.

Absolute intensities

$$S_{n''n'} = \frac{8\pi^3 \nu N g_{n''} (1 - e^{-h\nu/kT}) e^{-E''/kT}}{3hc \sum_n g_{n''} \exp(-E''/kT)} |\langle n''|M|n'\rangle|^2$$

rare ab initio computations

– reproduce the order of magnitude

generally:

$$S_{n''n'} = C\, e^{-E''/kT} |\langle n''|M|n'\rangle|^2$$

The line parameters are obtained by combining experimental data with theoretical computations

two types AFGL : H_2O, CO_2, O_3, N_2O, CO, CH_4, O_2 and several trace constituents

GEISA: extension of AFGL

about 300 000 lines

Line shape

$$k(\nu) = S\, f(\nu-\nu_0)$$

$$\int_{-\infty}^{+\infty} f(\nu-\nu_0)\, d\nu = 1$$

Doppler $\Delta\nu = \frac{v}{c}\nu_0$

$$p(v) = \left(\frac{m}{2kT}\right)^{1/2} \exp\left(\frac{-mv^2}{2kT}\right)$$

$$f(\nu-\nu_0) = \frac{1}{\alpha_D\sqrt{\pi}} \exp\left\{-\left(\frac{\nu-\nu_0}{\alpha_D}\right)^2\right\}$$

$$\alpha_D = \frac{\nu_0}{c}\left(\frac{2kT}{m}\right)^{1/2}$$

Lorentz or natural

$$f(\nu-\nu_0) = \frac{1}{\pi}\frac{\alpha_N}{(\nu-\nu_0)^2+\alpha_N^2}$$

$$\alpha_N = \frac{1}{4\pi\phi_c} \quad \text{natural case}$$

Voigt: $f(\nu-\nu_0) = f_{Dop} * f_{Lor}$

Van Vleck – Weisskopf

$$f(\nu) = \frac{1}{\pi}\left(\frac{\nu}{\nu_0}\right)^2\left(\frac{\alpha_L}{(\nu-\nu_0)^2+\alpha_L^2} + \frac{\alpha_L}{(\nu+\nu_0)^2+\alpha_L^2}\right)$$

$$W(nl) = \int_{-\infty}^{+\infty} A_\nu\, d\nu = \int_{-\infty}^{+\infty} (1 - \exp(-k_\nu nl))\, d\nu$$

(30)

Whiting (1967) approximation to the Voigt profile

(31)

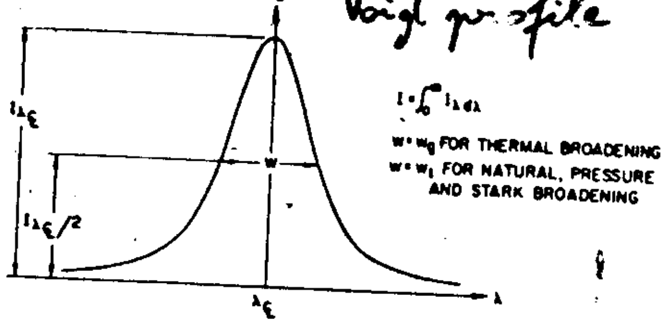

FIG. 1. Sketch of line profile.

Gaussian profile $I_\lambda = I_{\lambda_{\mathfrak{L}}} \exp -2.772(\lambda - \lambda_{\mathfrak{L}}/w_g)^2$.

Lorentzian profile $I_\lambda = I_{\lambda_{\mathfrak{L}}} \dfrac{1}{1+4(\lambda-\lambda_{\mathfrak{L}}/w_l)^2}$.

$$w_v = \frac{w_l}{2} + \sqrt{\left(\frac{w_l^2}{4} + w_g^2\right)}.$$

$$\frac{I_\lambda}{I_{\lambda_{\mathfrak{L}}}} = \left[1 - \frac{w_l}{w_v}\right] \exp\left[-2.772\left(\frac{\lambda-\lambda_{\mathfrak{L}}}{w_v}\right)^2\right] + \left[\frac{w_l}{w_v}\right]\frac{1}{1+4(\lambda-\lambda_{\mathfrak{L}}/w_v)^2}$$
$$+0.016\left[1-\frac{w_l}{w_v}\right]\left[\frac{w_l}{w_v}\right]\left\{\exp\left[-0.4\left(\frac{\lambda-\lambda_{\mathfrak{L}}}{w_v}\right)^{2.25}\right] - \frac{10}{10+(\lambda-\lambda_{\mathfrak{L}}/w_v)^{2.25}}\right\}.$$

$$I_{\lambda_{\mathfrak{L}}} = \frac{I}{w_v[1.065 + 0.447(w_l/w_v) + 0.058(w_l/w_v)^2]}$$

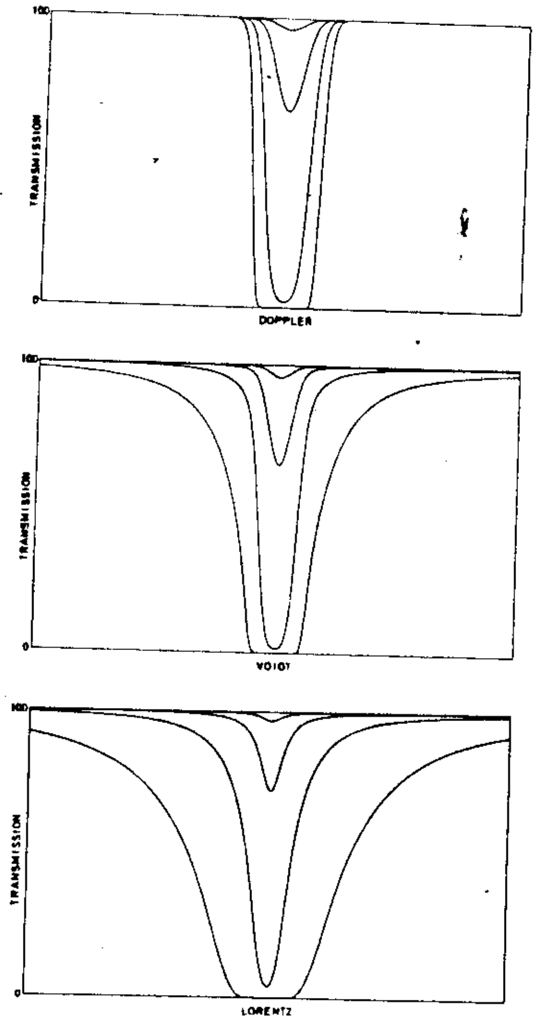

Fig. 3.2. Comparison between the Lorentz, Doppler and Voigt profiles, the optical path being multiplied each time by a factor of 10.

Line by line computation

- define a frequency net
  - computation step $< \frac{1}{3} \alpha_{min}$
  - subline positions should absolutely not be systematically points

- problem very similar to numerical integration.
- A variable step is possible !!!

- define an altitude net
  - optical path in the layers should be equivalent.

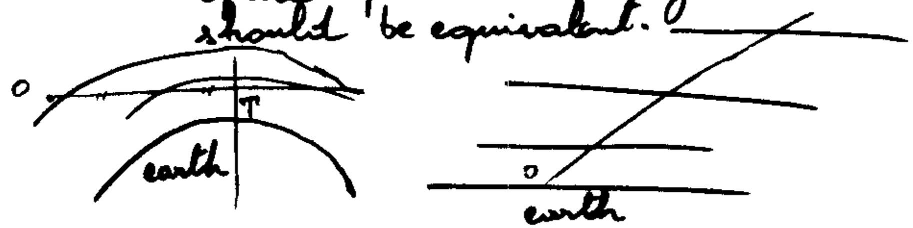

- include all lines of all intervening constituents
  Add at each frequency point all the k's corresponding to lines and altitudes
- compute corresponding transmission
- introduce instrument or filter function

(34)

Band models

Theoretical considerations

$$k_\nu = \sum_{i=1}^{i=n} \frac{S_i}{\pi} \frac{\alpha_i}{(\nu-\nu_i)^2+\alpha_i^2}$$

equally spaced lines δ, same α_L, same S

$$k_\nu = \sum_{i=-\infty}^{i=+\infty} \frac{S}{\pi} \frac{\alpha_L}{(\nu-i\delta)^2+\alpha_L^2}$$

Elsasser model $\quad y = \frac{\alpha_L}{\delta} \quad x = \frac{\nu}{\delta}$

$$u = \frac{S w}{2\pi \alpha_L}$$

$$y \to \infty \to W = 1 - e^{-\frac{S w}{\delta}}$$

$$y \to 0 \quad \bar{A} = 2\pi y L(u)$$

L: tabulated function (Ladenburg and Reiche)

$$y \ll 1 \to W = 1 - \mathrm{erf}(\pi y \sqrt{2u})$$

Practically

15 μm CO_2 band:

troposphere:

$$W = 1 + 0.27 - 0.22 \log[w(p+p')]^{0.88}$$ (with p' = partial pressure)

$$W = 1 - 10^{(1.44 - 0.309 w^{-0.237})}$$

higher levels: $W = 1 - \exp(0.32 w^{0.4})$

(35)

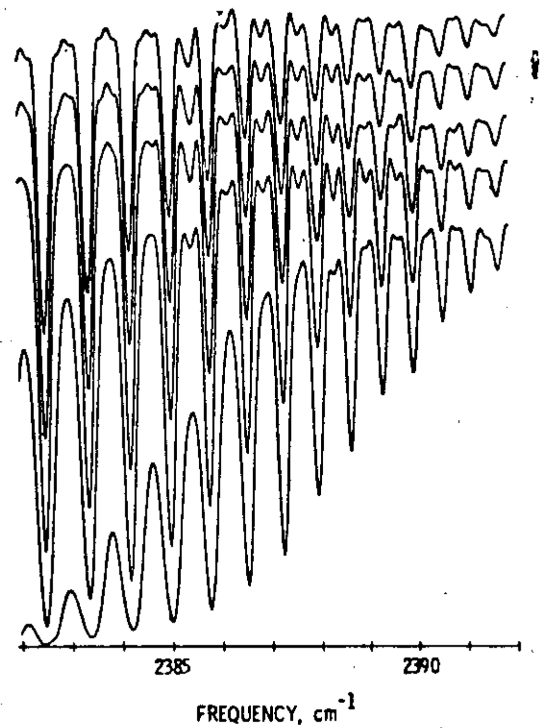

Figure 14-A

Farmer et al.

Curve of growth : influence of the Lorentzian wings.

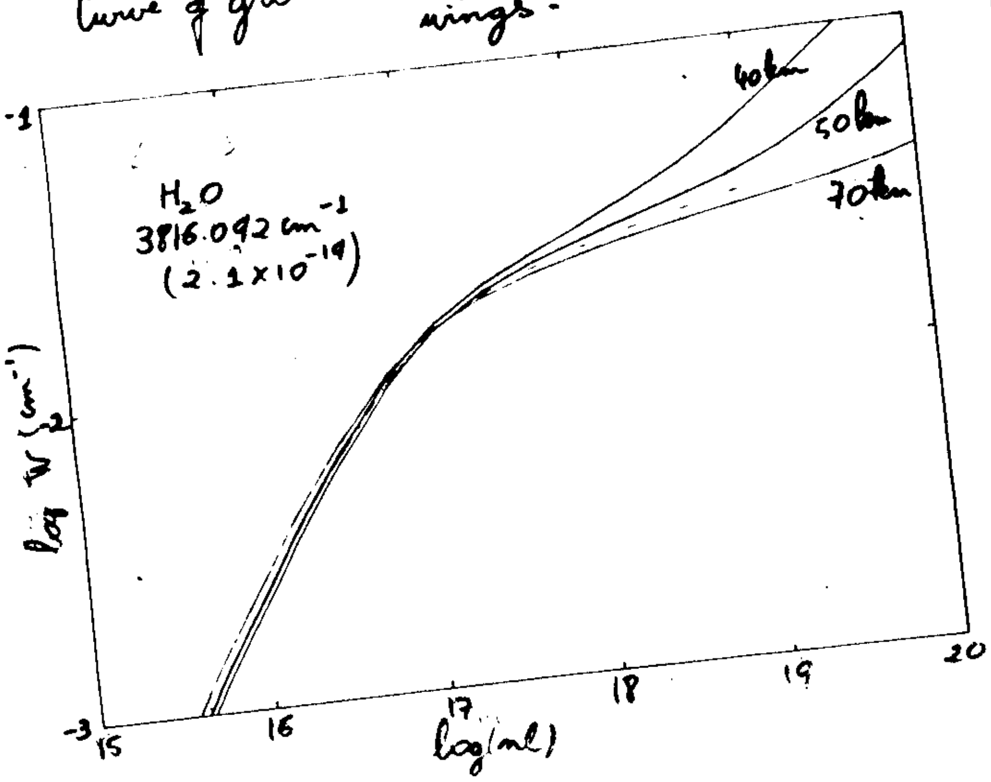

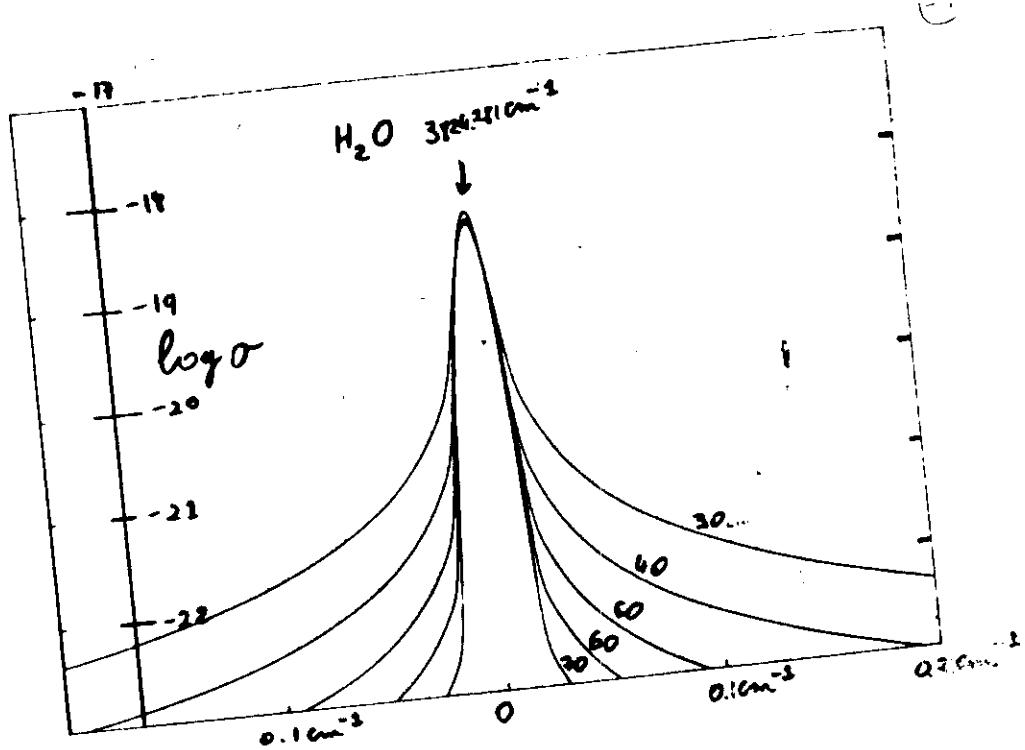

Saturation phenomenon:

the Dopplerian core is almost constant with altitude.

the changes in absorption coefficients are in the Lorentzian wings.

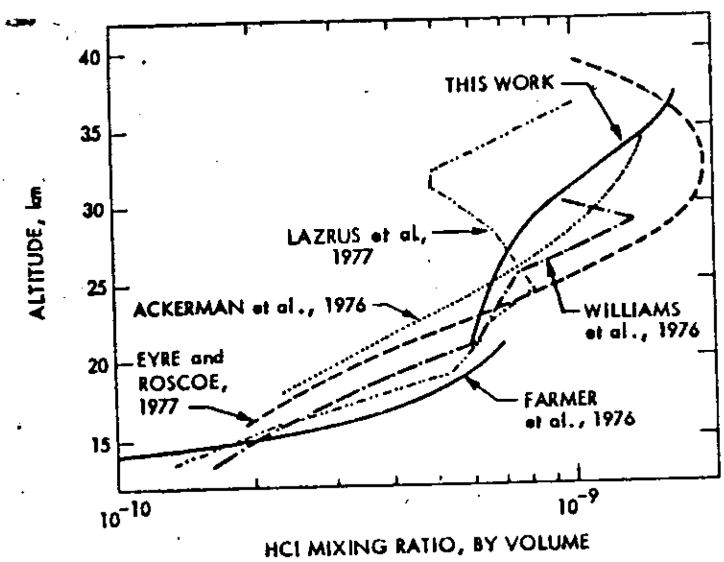

Figure 9

Farmer et al.

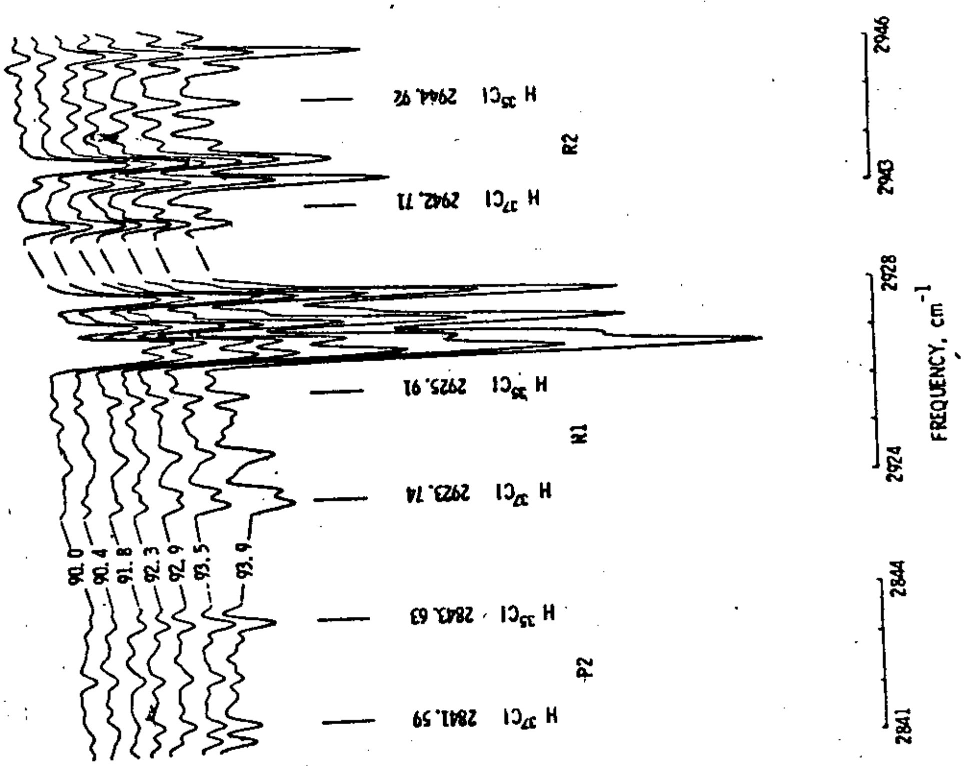

Figure 6

Farmer et al.

REMOTE SENSING by EMISSION TECHNIQUES

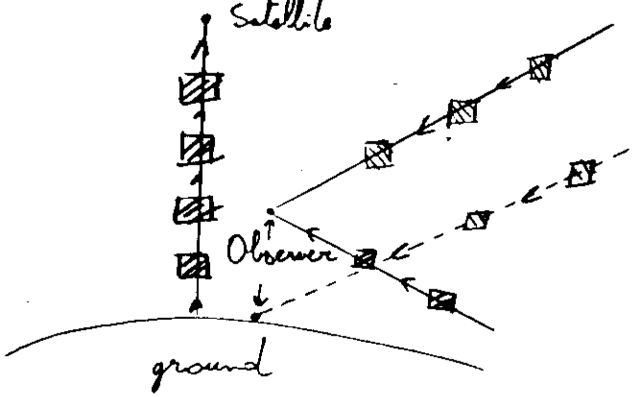

Atmospheric emissions limiting blackbody $\left\{ \begin{array}{l} M = \sigma T^4 \\ \lambda_M = \left(\frac{2897.5}{T}\right) \mu m \end{array} \right.$

Emission of an element of air:

$$M_\nu = (1 - T_\nu) M_\nu^{BB}$$

T_ν : transmission : $T_\nu = \frac{I_\nu}{I_0} = e^{-k_\nu n l}$

An element is chosen as optically thin:

$$e^{-k_\nu n l} = 1 - k_\nu n l$$

$$\rightarrow M_\nu = k_\nu n l B_\nu$$

Perfect linear case

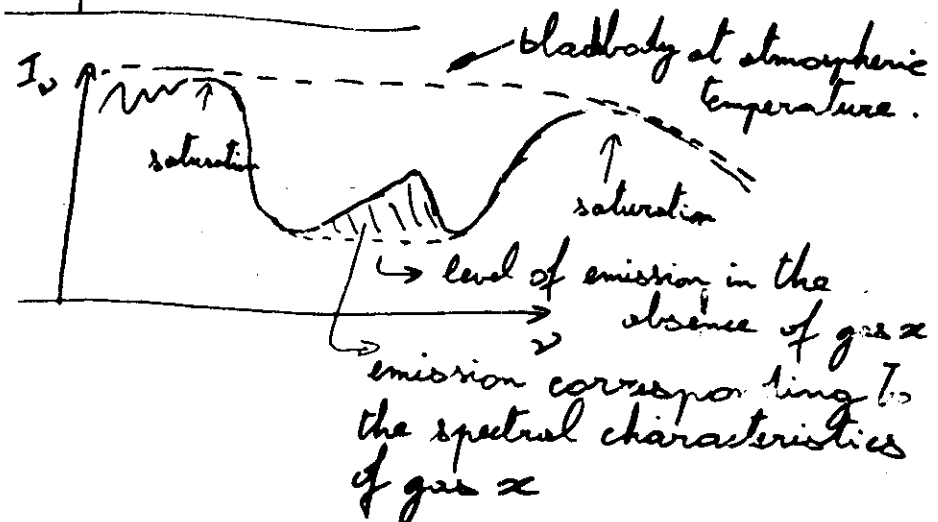

In this very special case : $\frac{M_\nu}{B_\nu} = k_\nu n l$

direct determination of nl.

→ usually not the case

Inversion of radiative transfer equations

$$\left\{ \begin{array}{l} E_1(\nu) = k_1(\nu) n_1 l_1 B_1(\nu) \\ E_2(\nu) = E_1(\nu) e^{-k_2(\nu) n_2 l_2} + k_2(\nu) n_2 l_2 B_2(\nu) \\ \text{- - - - - - - - -} \\ E_i(\nu) = E_{i-1}(\nu) e^{-k_i(\nu) n_i l_i} + k_n(\nu) n_n l_n B_n(\nu) \end{array} \right.$$

unknowns: either n_i or T_i (correspond to B_i)

[redacted]

Infrared emission

Rotation-vibration : same spectra appear in absorption.

differences: temperature effects
→ much greater importance of continua.
→ line wings of warm gases
→ a possibility to infer vertical distributions with the knowledge of temperature profile.

Best region: around 10 μm
no scattering of sun or moonlight
could be performed day or night

day observations: the sun should not be in the field of view.

Geometry: choosen by the observer.
limb sounding

(16) Problems related to infrared emission

- Weak signal { T: 300 K compared to 6000 K
  - necessitates much better detectors
  - would necessitate coaddition of spectra.
  - If we had perfect detectors: a cryogenically cooled instrument would be necessary.
- Practically: filter instruments with controlled references
  interferometers calibrated on a cold blackbody
- Soon: cryogenically cooled high resolution spectrometers.
- From space: - the grille spectrometer will attempt the observation of thermal emission
  - most of its planned emission modes will however be directed towards the thermosphere.

Microwave

Sub mm : 300 — 3000 GHz : 100 μm [illegible]
mm range : $\nu < 300$ GHz : 1 [illegible]

A different spectroscopy:

the frequency of the lines is simply given by the difference in energy between two consecutive rotational states:

diatomic: $\nu = 2B(J+1)$ $B = \frac{h}{8\pi^2 I}$

! the spacing of few lines gives directly 2B

Direct access to rotational constants for the other types of molecules.

line shape: much lower frequency: Doppler 100 times narrower

at 300 GHz for O_2:

ground level: $\alpha_L = 0.3$ GHz, $\alpha_D = 3.2 \times 10^{-4}$ GHz

$\alpha_L = \alpha_D$ at 1 mb: 45 km

Microwave geometries

- uplooking: the sensor is below the atmospheric layer

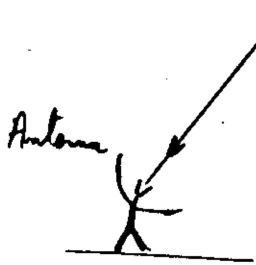

[optically thin part of the spectrum
↓
measured resonance line shape by heterodyne technique
resolution ≃ 10 km, up to mesosph[ere]

- nadir looking

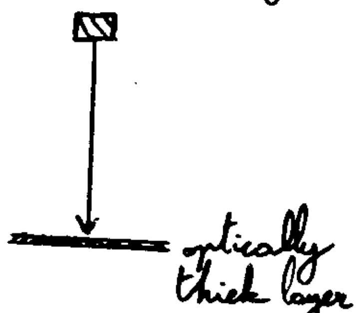

- either the same principle as uplooking: necessitates a good knowledge of the background
  NIMBUS 5, 6 and 7: total H_2O over ocean.
- or optically thick case: very similar to CO_2 temperature soundings.

- limb sounding: most promising technique, will be tried from EOM.

Advantadges of µwave

- unsensitive to clouds
  aerosols
  must only be interrupted during precipitations (same principle as a meteorological radar)
- much less cluttered than the infrared.
- in most cases: Lorentz up to the mesosphere
- No non LTE effects in the middle atmosphere.
- Frequency resolution is practically unbounded.
- Permits the simultaneous observation of H_2O, ClO, CO, O_3 and O_3; O_2 giving temperature.
- the line width as a strong function of altitude permits altitude Resolution.

Radiative transfer and inversion.

- very far from blackbody maximum
  Rayleigh-Jeans approximation
  radiated power $\approx T$
  and not T^4

Inversion techniques

- A model is fitted to find the corresponding resonance line.
- Statistical method based on a well known a priori statistics of the parameter to be investigated. An inversion matrix is calculated by multidimentional regression to minimize the error between the original parameter and the retrieved parameter distribution
- Iterative methods (Chahine)

Main spectroscopic problems

- line shape
- line width

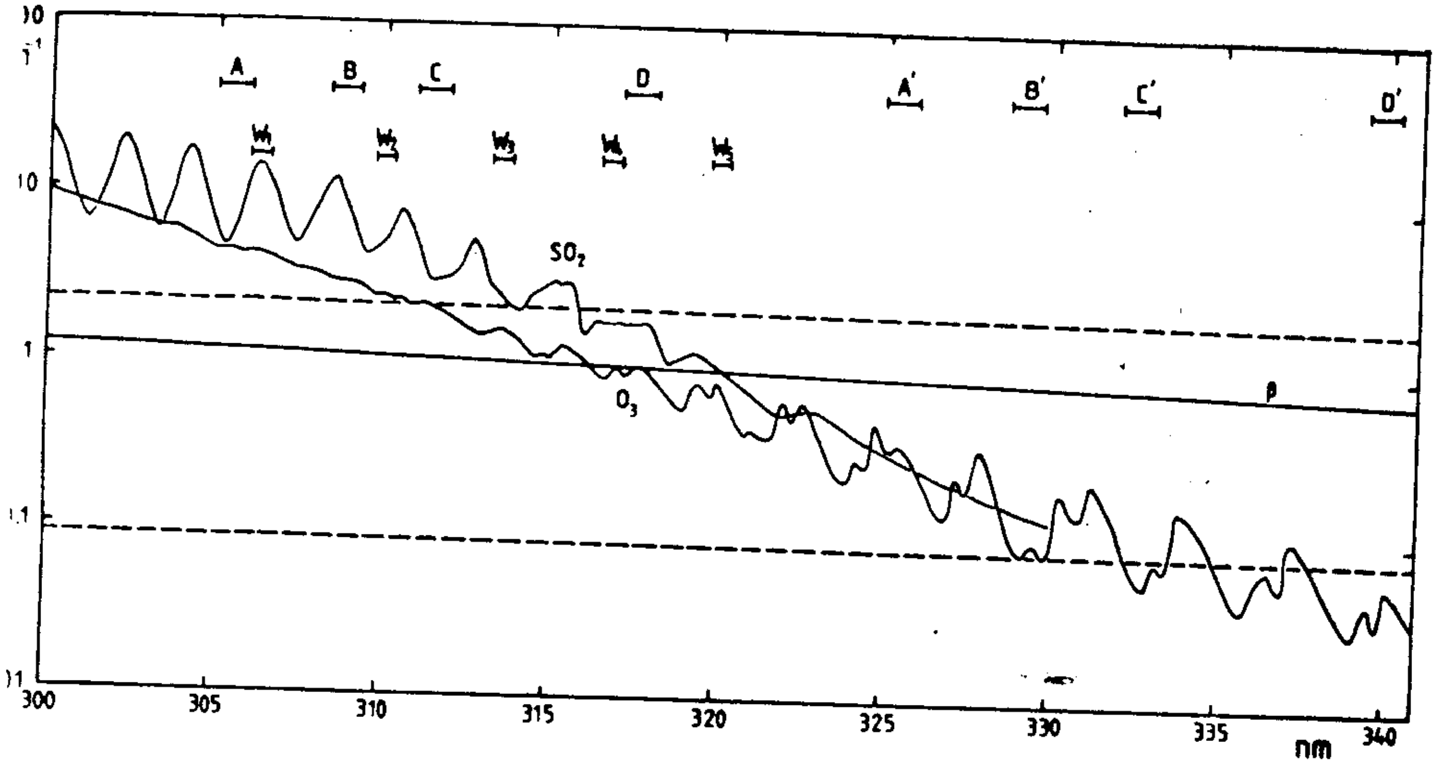

52

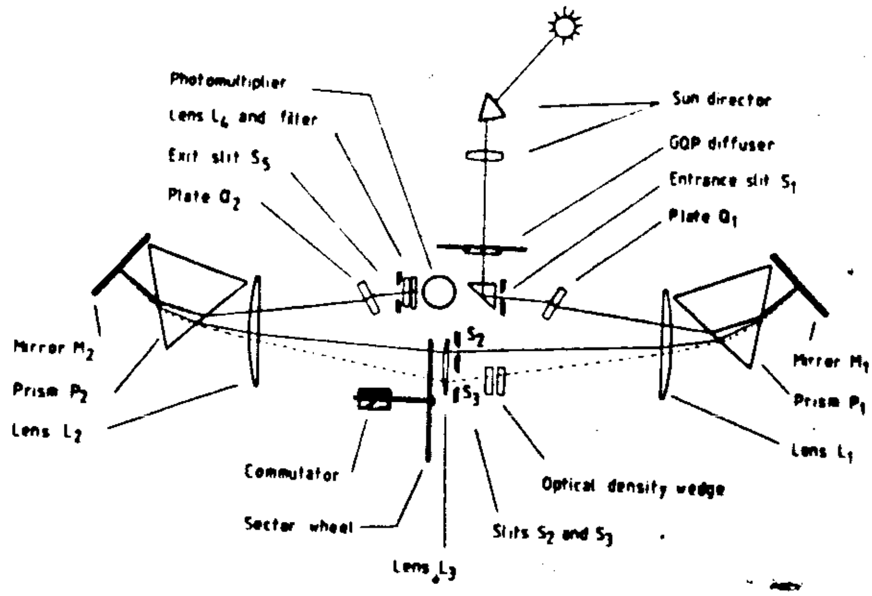

Figure 1.2 Schematic diagram of the main optical and mechanical parts of the Dobson spectrophotometer.

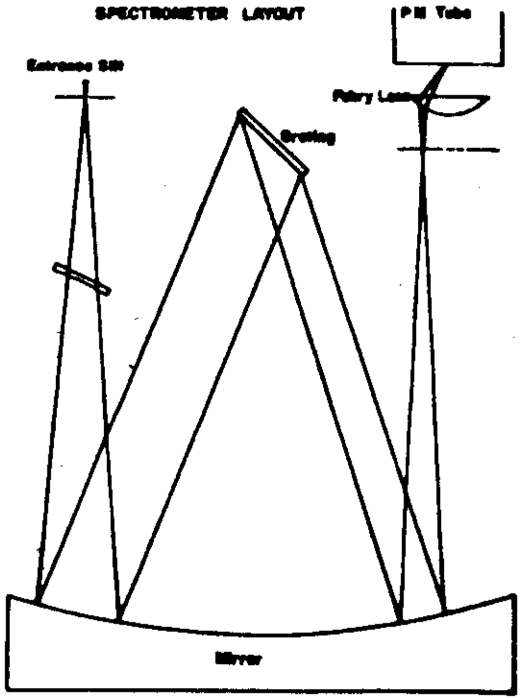

Fig. 1: The optical layout of the grating spectrophotometer

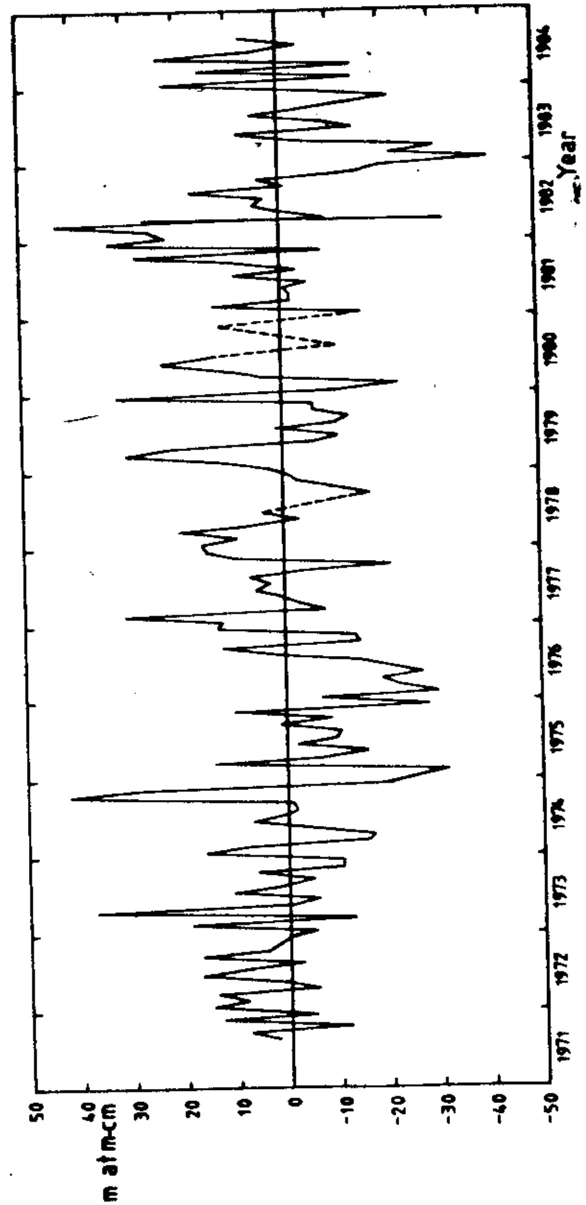

Space borne infrared absorption

historical milestones

- around 1960: aircraft flights of low resolution [illegible]
- 1963: (Houghton) limb sounding projects
- 1967-1972:
  - Cumming-Lowe 1 cm^{-1}
  - IASB 2 cm^{-1}
  - MURCRAY et al 0.3 cm^{-1}
  - discoveries of NO_2 and HNO_3
  - Zander : 0.03 cm^{-1}
- 1973-1980:
  - grille spectrometer 0.1 cm^{-1}
  - J.P.L. mark 1 0.15 cm^{-1}
  - Zander (limb sounding)
  - high resolution interferometer: Murcray et al, Buijs et al
  - discoveries of NO, HCl, HF
- 1983: first space flight of the grille spectrometer
- 1985: ATMOS flight
- 1985-?: 20 ATMOS flights in combination with the grille spectrometer or other instruments.

Limb sounding geometry

① balloon:

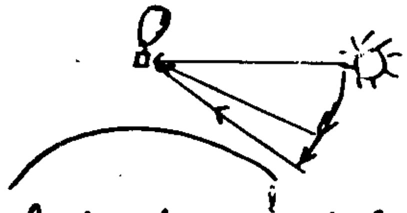

an observer, relatively immobile vs the earth, uses the earth rotation to see the Sun occulted by atmospheric layers at lower altitudes.

Altitude of the grazing ray:

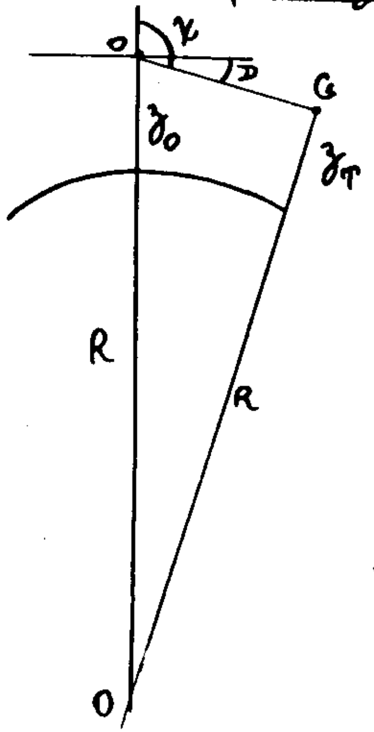

$$(R+z_0)\cos\chi = R + z_T$$

$$z_T = (R+z_0)\cos(\chi - \tfrac{\pi}{2}) - R$$

$$z_T = 0 \Rightarrow \cos D = \frac{R}{R+z_0}$$

refraction: negligible above 20 km altit

Sun loss: 10-15 km altitude.

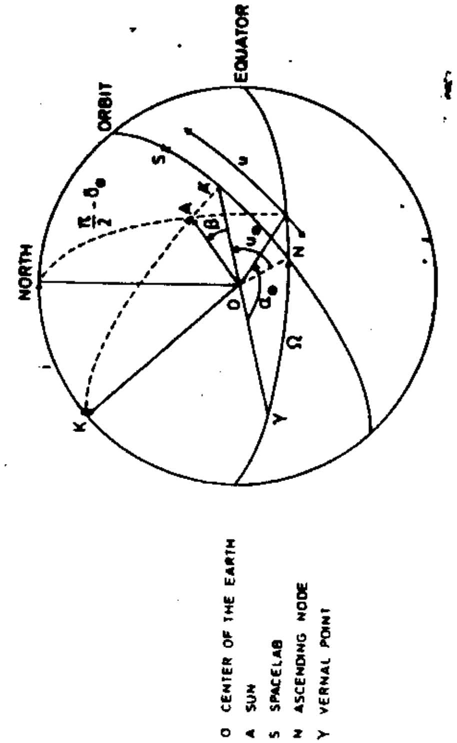

Fig. 2

D) Satellite :

an observer, in orbital motion around the earth, uses its own motion to see the Sun occulted by atmospheric layers at lower altitudes.

- the earth rotation does not define anymore the times of sunrise and sunsets.

Condition for occultation

β angle : angle between the solar vector OA and its projection in the orbital plane OA'
(positive when the solar vector has a normal component to the orbital plane directed along the angular momentum vector of the satellite)

. $\cos\beta > \sin D \Rightarrow |\beta| < 90° - D$

250 km : $D_{max} \simeq 16° \rightarrow |\beta| < 74°$

500 km : $D_{max} \simeq 22° \rightarrow |\beta| < 68°$

Otherwise : no terminator : full Sun orbit.

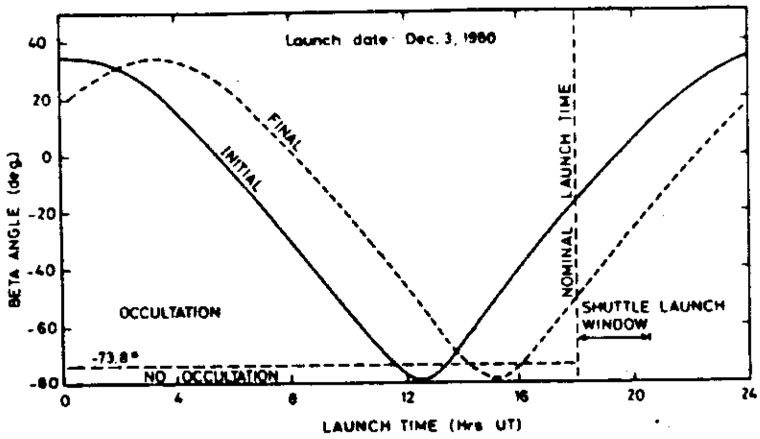
Launch date: Dec. 3, 1980
BETA ANGLE (deg.)
LAUNCH TIME (Hrs UT)
INITIAL
FINAL
NOMINAL LAUNCH TIME
SHUTTLE LAUNCH WINDOW
OCCULTATION
-73.8°
NO OCCULTATION

Fig 3

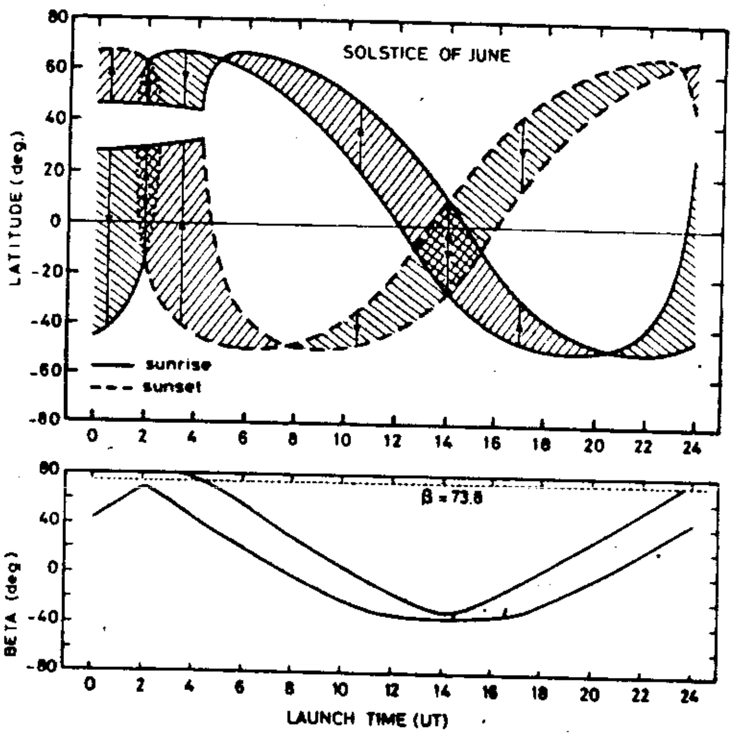
SOLSTICE OF JUNE
LATITUDE (deg.)
sunrise
sunset
BETA (deg)
β = 73.8
LAUNCH TIME (UT)

Fig. 7

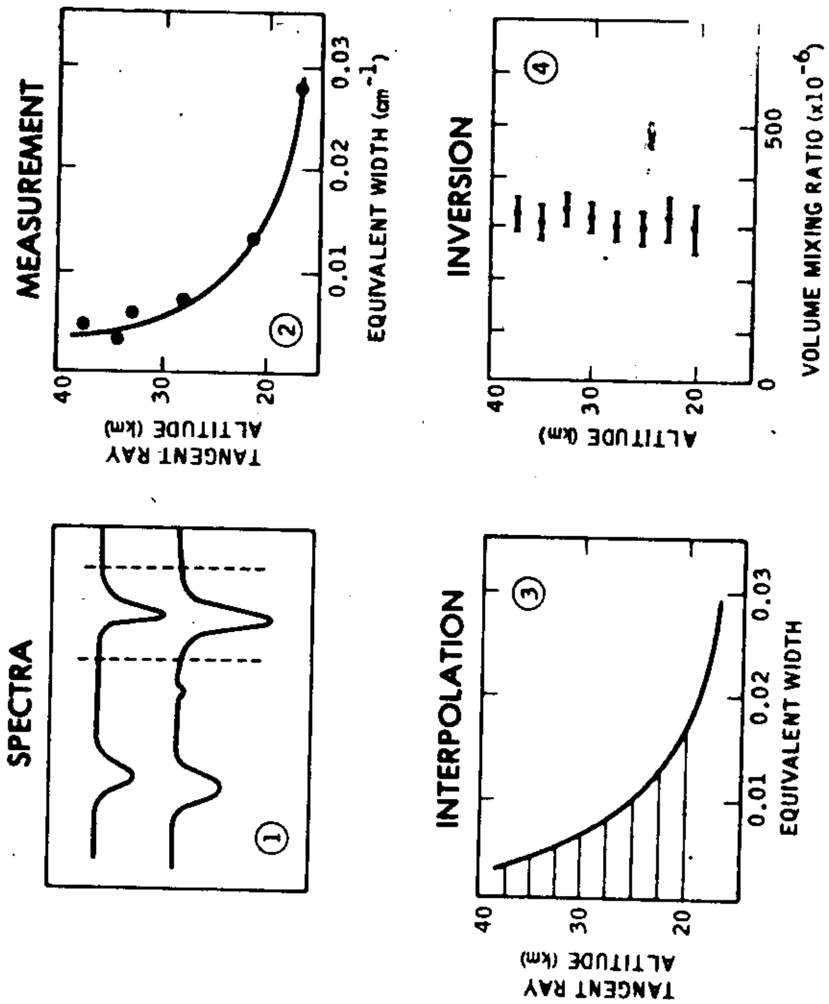

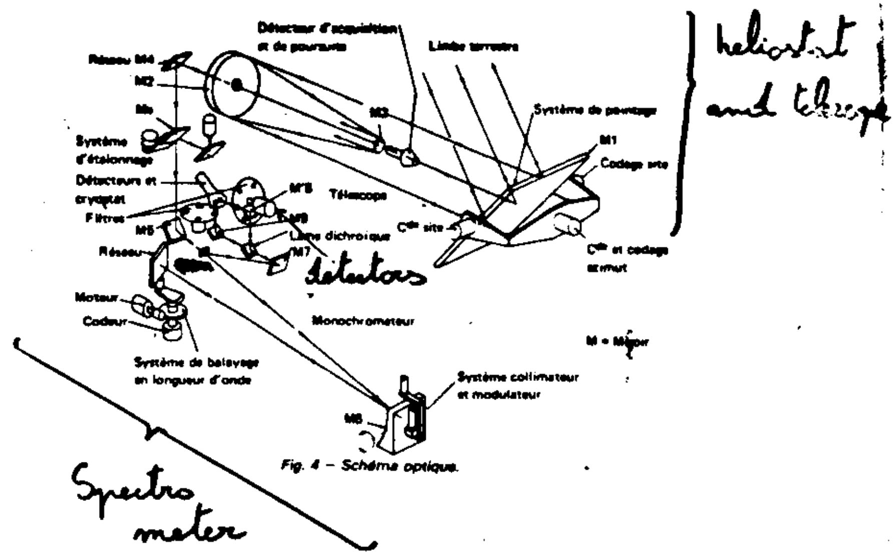

Fig. 4 – Schéma optique.

the grille in the spectrometer replaces the entrance and exit slits.

two detectors : In Sb
Hg Cd Te

Spectral windows

grating angles
settings of the filter wheel
gains of the detectors

64 windows : 40 numbered 24 to 63 are fixed
24 : 0 to 23 are programmed

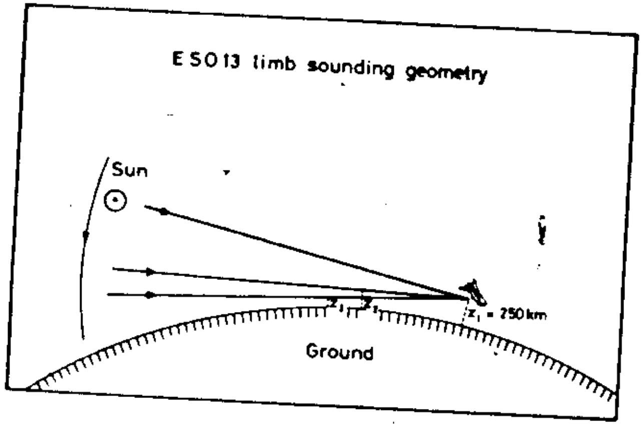

Fig. 4.1 Limb sounding geometry in the case of the Spacelab borne ES013 grille spectrometer.

Programs: 12 successive altitude zones to which corresponds one window (in fact, two successive windows are possible but this possibility has not been applied)

altitude zones: 250 Practically, the
200 sun has been
160 lost at 30 in
120 the Northern hemisphere,
100 around 20 in
80 the Southern
60 hemisphere
50
40
30
20
10